Efficient Training Phase for Ultra-Wideband based Location Fingerprinting Systems

Christoph Steiner and Armin Wittneben, *Member, IEEE*

Abstract

Location fingerprinting utilizing ultra-wideband radio frequency signals is an attractive alternative to conventional positioning concepts based on range, angle, or received signal strength estimates. Such a location fingerprinting method proves particularly beneficial in indoor environments with dense multipath propagation and non-line-of-sight situations where conventional approaches would fail. The ultra-wide bandwidth allows for location fingerprints with many degrees of freedom and thus gives the important advantage that a single anchor suffices for good localization performance. The downside is that a large amount of training data is usually required, which makes the training phase time-consuming and tedious. In this paper, we propose and study a novel and efficient training method which is based on the idea of spatial signal prediction. We develop a regional channel model which supports spatial signal prediction in the vicinity of a reference point. We show that the parameters of this regional channel model can be estimated from very few measured received signals with known transmitter and receiver positions. The prediction accuracy and the location fingerprinting performance are evaluated with measured channel impulse responses obtained in an anechoic chamber and in a typical office environment.

Index Terms

Ultra-Wideband, Location Fingerprinting, Training, Prediction, Channel Model

Christoph Steiner was with the Communication Technology Laboratory, ETH Zurich, and is now with Infineon Technologies Austria AG, Babenbergerstr. 10, 8010 Graz, Austria (email: christoph.steiner@infineon.com). Armin Wittneben is with the Communication Technology Laboratory, ETH Zurich, 8092 Zurich, Switzerland (email: wittneben@nari.ee.ethz.ch).

The authors would like to thank Dr. Juergen Kunisch from IMST GmbH, Kamp-Lintfort, Germany for providing ultra-wideband channel impulse response measurements.

I. Introduction

Location fingerprinting [1], [2], [3], [4] is a promising alternative to conventional localization approaches like multilateration or multiangulation [5], [6]. Especially in harsh propagation environments with many multipaths and non-line-of-sight (non-LoS) conditions, the application of such conventional techniques is limited. The existence (detectability) of the LoS path (direct path) is a prerequisite for the usability of a radio link for multilateration or multiangulation. In contrast, location fingerprinting techniques do not rely on the existence of the direct path. Furthermore, the multipath structure of the propagation channel provides significant location information, since it depends on the positions of transmitter and receiver. Location fingerprinting schemes are able to utilize multipath information, provided that the radio frequency (RF) signal bandwidth is large enough. Consider, for example, a narrowband communication system which employs received signal strength (RSS) as location fingerprint. Such a system offers only one degree of freedom (one RSS value) per anchor. Hence, a large number of anchors and communication among those anchors are required. On the contrary, ultra-wideband (UWB) signals exhibit already many degrees of freedom, which imply that a single anchor suffices to achieve good localization performance [4]. This is essential for many applications such as self-localization of nodes in an ad-hoc wireless network [7], which operate without pre-installed infrastructure.

Location fingerprinting is particularly suited for applications, where the positions of agents are restricted to certain regions of space. Furthermore, it should be sufficient for the application to merely detect the current region of an agent instead of providing exact coordinates. An illustrative application example is a tire pressure monitoring system (TPMS), which warns the driver of a vehicle that the pressure in a tire exceeds the specified limits. Modern TPMS provide also the specific location of the tire (e.g. front right) together with the corresponding pressure value. Among the numerous methods for tire localization[1], there exist also RF based approaches, which utilize the wireless communication links between pressure sensors on the wheels and an on-board receiver. Location fingerprinting is the method of choice here, since the application has to decide only between four possibilities (front right, front left, rear right, rear left). Moreover, conventional RF based methods would fail because of non-LoS and dense multipath conditions.

Another application example is equipment tracking in an office building, laboratory, or

[1]Note that tire localization via identification numbers is insufficient, because wheels can be relocated.

hospital. Working areas (e.g. desks) define the allowed regions, where the equipment (e.g. oscilloscope) can be located. The actual region of the equipment item is detected via location fingerprinting utilizing RF communication links to fixed receivers (e.g. WIFI access points). Additional status information could indicate by whom this item is currently used and how long it will be allocated.

In general, location fingerprinting systems consist of two phases. During the training phase, the system gathers location fingerprints from known positions. During the localization phase, location fingerprints from agents with unknown positions are observed and matched to the training data. There exists a large number of methods for this pattern matching such as support vector machines, neural networks, weighted k nearest neighbors, or Bayesian approaches [8], [9]. The performance is mainly determined by the training effort, the choice and statistical modeling of the location fingerprints, the classification algorithm, the signal-to-noise ratio (SNR) of the RF signals, the variability of the propagation environment, and the number of anchors. Besides performance, low complexity is a key requirement for a ubiquitous and practicable application of such location fingerprinting systems. The overall complexity is usually dominated by the complexity of the training phase, where information about the propagation environment is obtained by supervised channel measurements. This task is generally very time-consuming and, moreover, has to be repeated if the propagation environment changes.

The main contribution of this paper is a novel and efficient training method for location fingerprinting systems, which requires only very few supervised channel measurements per region. We show that channel impulse responses can be spatially predicted in the vicinity of a reference point based on only very few measured channel impulse responses. Applying this prediction method, arbitrarily many training signals can be generated without the need for expensive and time-consuming measurements. Other important contributions of this paper are the experimental confirmation of the proposed prediction method and a comprehensive experimental performance evaluation.

The paper is structured as follows. Section II gives a detailed problem description. We develop the required theory and introduce the parameterized regional channel model in Section III. Section IV is concerned with the estimation of the parameters of this regional channel model. Section V demonstrates how predicted training signals are used by the location fingerprinting system during the training phase and Section VI presents the experimental performance analysis.

II. Problem Statement

We consider an indoor scenario and a given surveillance area which subsumes all possible agent positions. Note that the surveillance area does not have to be a connected set. Depending on the application, as for example for TPMS or equipment tracking, isolated regions are sufficient. The agents are wireless devices which can send and receive RF signals with an ultra-wide bandwidth. A wireless device with known and fixed position acts as single anchor. The surveillance area is separated into M regions. Here, it is important to realize that the number of regions and their dimensions are determined by the application. In case of TPMS only four regions with circular ring shape are relevant. In case of equipment tracking there might exist up to fifty regions with various shapes.

The location fingerprinting system should detect the region in which an agent under test is currently located based on the observed RF signal at the anchor[2]. Hence, this localization problem is equivalent to a hypothesis testing problem. The performance is measured with the average classification error probability $\mathcal{P}_e$ defined as

$$\mathcal{P}_e \triangleq \sum_{j=1}^{M} \pi_j \sum_{i=1, i\neq j}^{M} p_{i,j}, \tag{1}$$

where $p_{i,j}$ denotes the probability of deciding for region i, when the agent is located in region j. The a priori probabilities of the hypotheses are denoted by $\pi_1, \pi_2, \ldots, \pi_M$. The average error probability $\mathcal{P}_e$ is a suitable and accessible measure for a relative comparison of different solution methods. However, a complete performance characterization would consist of the distribution of classification errors over all regions.

A location fingerprint vector is denoted by $\mathbf{y}$ with length I. It is extracted from the observed RF signal at the anchor. For example, $\mathbf{y}$ could consist of complex samples of a channel impulse response in equivalent baseband representation, where the vector length I and the sampling frequency determine the signal observation time. The vector $\mathbf{y}$ is modeled by a parameterized probability density function (PDF) denoted by $f(\mathbf{y}|\Theta_m)$. The parameters Θ_m of this PDF are deterministic and distinguish different regions. Consequently, the problem of deciding in which region the agent under test is located based on $\mathbf{y}$ is formulated as a Bayesian M-ary

[2]This setup corresponds to remote positioning. If the region is detected based on RF signals observed at the agent from the anchor, this is called self-positioning. In the following, we consider only remote positioning but all concepts and algorithms carry over to self-positioning.

hypothesis testing problem [10]. The decision rule minimizing $\mathcal{P}_e$ is given by

$$\hat{m} = \underset{m=1,2,\ldots,M}{\operatorname{argmax}} \pi_m f\left(\mathbf{y}|\Theta_m\right). \tag{2}$$

During the training phase, the parameters Θ_m have to be estimated for all regions, i.e. for $m = 1, 2, \ldots, M$. The number of free real parameters in Θ_m is a function of the vector length I, which is denoted by $h\left(I\right)$. For example $h\left(I\right) = I^2$, if Θ_m is the covariance matrix of a circular symmetric Gaussian PDF. Assume that we have J measured training vectors from region m for the estimation of Θ_m available. As a rule of thumb, the number J should be at least as large as $h\left(I\right)$, such that the parameter estimates become accurate [9]. Hence, if $h\left(I\right)$ grows large, then up to now it has been necessary to collect a lot of supervised measurements for parameter estimation. In this work, we present a novel method for the estimation of Θ_m requiring only a very small number of measurements which is independent of $h\left(I\right)$.

III. Channel Models

When developing a channel model, it is essential to have its purpose in mind. If the channel model should describe propagation in general environments (e.g. office, factory, etc.) for communication system design, then site-independent parameterized statistical models [11] are required. A prominent example of such statistical channel models is the IEEE 802.15.3a channel model, which is based on the Saleh-Valenzuela channel model [12].

In this work however, we seek for spatial signal prediction based on measured signals from specific locations. Hence, we require a parameterized deterministic description of the received signals. The received signals could be calculated by solving Maxwell's equations. However, such computations require the knowledge of the electrical parameters of all materials in the environment, all location dependent boundary conditions and a lot of processing power to solve partial differential equations. Fortunately, such high modeling accuracy is not necessary for most engineering problems. A mathematically convenient simplification of Maxwell's equations is the multipath approximation based on the high-frequency approximation of electromagnetic wave propagation [13]. Its simplest form is called geometrical optics, where it is assumed that the electromagnetic field is composed out of partial waves traveling along geometric propagation paths (rays) and experiencing propagation effects during interaction with objects in the environment. This model provides accurate results as long as the interacting objects are electrically large, i.e. their dimensions are larger than the considered wavelengths. Furthermore, their electrical properties should remain approximately constant

for the wavelengths under study. The wavelengths used by UWB systems range from 3 cm up to 10 cm, which implies that for example walls, windows, floors, ceilings, and furniture can be considered as electrically large interacting objects.

A. Deterministic Multipath Channel Model

We consider a coordinate system where the position of the anchor is at the origin. The position of an agent acting as transmitter is denoted by $\mathbf{p} \triangleq [x, y, z]^T$. Applying the multipath approximation, we obtain an input-output relation between the transmitted signal $s(t)$ and the received signal $r(t, \mathbf{p})$ according to

$$r(t, \mathbf{p}) = \sum_{l=1}^{L(\mathbf{p})} g_l(\mathbf{p})\, s(t - \tau_l(\mathbf{p})) + w(t), \tag{3}$$

where $L(\mathbf{p})$, $g_l(\mathbf{p})$ and $\tau_l(\mathbf{p})$ are the number of multipath components, the gain and the delay of the l-th path as function of $\mathbf{p}$. The signal $w(t)$ is a realization of a stochastic process which accounts for random disturbances like thermal noise. The impulse responses of transmit and receive antenna, filters, and amplifiers are comprised in $s(t)$. It is assumed that frequency dependent interactions, which cause distortions of the transmitted signal $s(t)$, can be neglected.

B. Parameterized Regional Channel Model

In this section, we develop a regional channel model, which describes the deterministic behavior of $r(t, \mathbf{p})$ as function of $\mathbf{p}$ in the vicinity of a reference point $\mathbf{p}_0$. If we think about a location fingerprinting application, then this reference point must be located somewhere within a region.

1) Path Gains: The path gain $g_l(\mathbf{p})$ accounts for the loss in amplitude of the l-th partial wave due to the traveled distance and the l-th interacting object. These large scale effects vary on a much larger spatial scale than the path delays. Therefore, it is commonly assumed that the path gains stay approximately constant for small changes of $\mathbf{p}$ in the order of a few multiples of the carrier wavelength[3] [11], [14]. Consequently, we propose to approximate the path gains in the vicinity of $\mathbf{p}_0$ according to $g_l(\mathbf{p}) \approx g_l(\mathbf{p}_0)$.

[3]Note that fading due to multipath interference does not influence the individual path gains. This effect is caused after summation over all L multipath components.

2) Path Delays: In this section, the functional dependence of $\tau_l(\mathbf{p})$ on $\mathbf{p}$ and the l-th interacting objects is derived. The path index l is dropped in the following derivations for notational convenience.

Diffracting and scattering objects are described by the coordinates of the diffraction or scatter point denoted by $[x_d, y_d, z_d]$. The corresponding path delay is determined by the sum of the distances from agent to $[x_d, y_d, z_d]$ and from $[x_d, y_d, z_d]$ to the anchor according to

$$\tau(\mathbf{p}) = \frac{1}{c_0}\left(\sqrt{(x+a)^2+(y+b)^2+(z+c)^2}+\sqrt{a^2+b^2+c^2}\right),$$

with the propagation speed c_0 and $a=-x_d$, $b=-y_d$, and $c=-z_d$.

Reflecting objects are in general surfaces in the three-dimensional Euclidian space. Since we consider only small changes of $\mathbf{p}$, reflecting objects are approximated as planes. These are specified in the Hessian normal form with the normal vector $\mathbf{n} \triangleq [n_x, n_y, n_z]^T$ with unit norm and the vector $\mathbf{r}$ from the origin to an arbitrary point on the plane. The equation $\mathbf{n}^T(\mathbf{r}_p - \mathbf{r}) = 0$ defines a plane consisting of all points $\mathbf{r}_p$ fulfilling this equation. The smallest distance of $\mathbf{p}$ to this plane is given by $\left|\mathbf{n}^T(\mathbf{p}-\mathbf{r})\right|$. The image point $\mathbf{p}_\mathrm{I}$ of $\mathbf{p}$ is obtained by mirroring $\mathbf{p}$ on the reflecting plane according to

$$\mathbf{p}_\mathrm{I} = \mathbf{p} + \left(2\mathbf{n}^T(\mathbf{p}-\mathbf{r})\right)\mathbf{n}.$$

The distance of the image point to the origin (anchor) is the same as the distance from $\mathbf{p}$ via reflecting plane to the origin. The corresponding path delay is therefore given by $\tau(\mathbf{p}) = \frac{1}{c_0}\|\mathbf{p}_\mathrm{I}\|$. Performing algebraic manipulations, the path delay equation is obtained as

$$\tau(\mathbf{p}) = \frac{1}{c_0}\sqrt{(x+a)^2+(y+b)^2+(z+c)^2}, \tag{4}$$

with $a=-2n_x\left(\mathbf{n}^T\mathbf{r}\right)$, $b=-2n_y\left(\mathbf{n}^T\mathbf{r}\right)$, and $c=-2n_z\left(\mathbf{n}^T\mathbf{r}\right)$.

It can be concluded from these derivations that the path delays can be written as

$$\tau(\mathbf{p}) = \frac{1}{c_0}\left(\sqrt{(x+a)^2+(y+b)^2+(z+c)^2}+d\right), \tag{5}$$

where d is either $\sqrt{a^2+b^2+c^2}$ for scattering and diffracting objects or zero for reflecting objects. Hence, the knowledge of the parameters a, b, c and the type of interacting object is sufficient to calculate the corresponding path delay for arbitrary agent positions. These parameters can be calculated from a floor plan or can be estimated from radar measurements [15], [16].

In this paper, we propose to utilize measured received signals at the anchor, which have been transmitted from known positions. It turns out that direct estimation of a, b, c and d is

a very complex task. In order to make the estimation problem feasible, we simplify (5) in the following.

3) Linearization of Path Delay Equation: Since we are anyhow interested in the behavior of the path delays as function of $\mathbf{p}$ in the vicinity of $\mathbf{p}_0$, it is reasonable to approximate (5) with a first order Taylor series expansion around $\mathbf{p}_0$ according to

$$\tau(\mathbf{p}) \approx \tau(\mathbf{p}_0) + [\alpha, \beta, \gamma](\mathbf{p} - \mathbf{p}_0) \tag{6}$$

with the linear coefficients α, β, and γ given by

$$\begin{aligned}
\alpha &= \frac{\partial \tau(\mathbf{p})}{\partial x}\Big|_{\mathbf{p}_0} = \frac{1}{c_0} \cdot \frac{x_0 + a}{\sqrt{(x_0+a)^2 + (y_0+b)^2 + (z_0+c)^2}}, \\
\beta &= \frac{\partial \tau(\mathbf{p})}{\partial y}\Big|_{\mathbf{p}_0} = \frac{1}{c_0} \cdot \frac{y_0 + b}{\sqrt{(x_0+a)^2 + (y_0+b)^2 + (z_0+c)^2}}, \\
\gamma &= \frac{\partial \tau(\mathbf{p})}{\partial z}\Big|_{\mathbf{p}_0} = \frac{1}{c_0} \cdot \frac{z_0 + c}{\sqrt{(x_0+a)^2 + (y_0+b)^2 + (z_0+c)^2}}.
\end{aligned} \tag{7}$$

The linear model in (6) unifies scattering and diffracting objects with reflecting objects. This means that all path delays in the received signal can be described by (6) irrespective of the interacting object and, moreover, the number of interactions. Furthermore, this linear model of the path delays is consistent with the plane wave assumption, i.e. assuming plane waves would lead to a path delay equation as in (6). We elaborate on this equivalence in the Appendix.

The parameterized regional channel model around $\mathbf{p}_0$ is obtained by inserting both aforementioned approximations in the input output relation in (3), which leads to

$$r_{\mathbf{p}_0}(t, \mathbf{p}) = \sum_{l=1}^{L(\mathbf{p}_0)} g_l(\mathbf{p}_0)\, s\left(t - \tau_l(\mathbf{p}_0) - [\alpha_l, \beta_l, \gamma_l](\mathbf{p} - \mathbf{p}_0)\right) + w(t), \tag{8}$$

where all geometrical parameters are collected in the set

$$\Psi_{\mathbf{p}_0} = \left\{ \{ g_l(\mathbf{p}_0), \tau_l(\mathbf{p}_0), \alpha_l, \beta_l, \gamma_l \}_{l=1}^{L(\mathbf{p}_0)} \right\}.$$

The knowledge of $\Psi_{\mathbf{p}_0}$ and the transmit signal $s(t)$ is sufficient to predict the disturbance-free signal at the anchor caused by an agent, which is located at an arbitrary point $\mathbf{p}$ in the vicinity of $\mathbf{p}_0$. The predicted signal is, of course, just an approximation to the true signal. There exist the following error sources:

1) The input output relation in (3) only approximates electromagnetic wave propagation. For example, distortions of the transmit signal $s(t)$ due to frequency dependent interactions are not accounted for in (3).

2) Path gains are assumed to be constant and path delays are approximated by a first order Taylor series expansion.
3) Errors in the estimation of $\Psi_{\mathbf{p}_0}$.

At this point, it is not clear which of these error sources have minor or major impact on the prediction accuracy and the location fingerprinting performance. In Section VI, we provide answers to these questions and give further insights with an extensive experimental performance analysis. But first, we turn our attention to the estimation of $\Psi_{\mathbf{p}_0}$.

IV. Estimation of Geometrical Parameters

A transmitter is positioned on a set of distinct measurement points $\mathbb{P} = \left\{\mathbf{p}_0, \mathbf{p}_1, \ldots, \mathbf{p}_{V-1}\right\}$ within a region and sends $s(t)$. The absolute coordinates of these measurement points are not required. Only the displacements of all measurement points relative to the reference point must be known. If the transmitter is equipped with a fixed antenna array and sends orthogonal (e.g. orthogonal in time) signals, then one supervised measurement per region is sufficient to obtain training data.

Sampled versions of the bandlimited received signals are observed at the anchor in a given time window and are normalized to unit energy. The received samples $r\left[n, \mathbf{p}_v\right]$ corresponding to position $\mathbf{p}_v$ are given by

$$r\left[n, \mathbf{p}_v\right] \triangleq r\left(nT_s, \mathbf{p}_v\right) = \sum_{l=1}^{L(\mathbf{p}_0)} g_l\left(\mathbf{p}_0\right) s\left(nT_s - \tau_l\left(\mathbf{p}_0\right) - \left[\alpha_l, \beta_l, \gamma_l\right]\left(\mathbf{p}_v - \mathbf{p}_0\right)\right) + w_v(nT_s)$$

with $n = 0, 1, \ldots, N-1$ and the sampling period T_s. The samples $w_v(nT_s)$ account for random disturbances like thermal noise. The problem of interest is the estimation of $\Psi_{\mathbf{p}_0}$ from $\left\{r\left[n, \mathbf{p}_0\right], r\left[n, \mathbf{p}_1\right], \ldots, r\left[n, \mathbf{p}_{V-1}\right]\right\}_{n=0}^{N-1}$ with known $\{s[n]\}_{n=0}^{N-1}$. Note that the reference point $\mathbf{p}_0$ is element of $\mathbb{P}$.

It is proposed to transform and solve this problem in the frequency domain, since the path delays and linear coefficients can take on only discrete values in the time domain, which are determined by the sampling period T_s. In order to increase the parameter estimation accuracy one would have to interpolate the time domain signals. In frequency domain, however, these parameters can take on any real number and T_s has only to fulfill the sampling theorem. Hence, the sampled received signals are transformed into the frequency domain by applying a unitary DFT yielding

$$R\left[k, \mathbf{p}_v\right] = S\left[k\right] \sum_{l=1}^{L(\mathbf{p}_0)} g_l\left(\mathbf{p}_0\right) \exp\left(-\imath \frac{2\pi k}{NT_s}\left(\tau_l\left(\mathbf{p}_0\right) + \left[\alpha_l, \beta_l, \gamma_l\right]\left(\mathbf{p}_v - \mathbf{p}_0\right)\right)\right) + W_v[k]$$

with $k = -\frac{N}{2}, \ldots, \frac{N}{2} - 1$ and $\{S[k]\}$ and $\{W_v[k]\}$ being the unitary DFTs of $\{s[n]\}$ and $\{w_v[n]\}$, respectively. For the estimation of $\Psi_{\mathbf{p}_0}$, we seek to minimize the following nonlinear least squares cost function

$$\mathcal{C}\left(\Psi_{\mathbf{p}_0}\right) = \sum_{v=0}^{V-1} \sum_{k=-\frac{N}{2}}^{\frac{N}{2}-1} \left| R[k, \mathbf{p}_v] - S[k] \sum_{l=1}^{L(\mathbf{p}_0)} g_l(\mathbf{p}_0) \exp\left(-\imath \frac{2\pi k}{NT_s} \left(\tau_l(\mathbf{p}_0) + [\alpha_l, \beta_l, \gamma_l](\mathbf{p}_v - \mathbf{p}_0)\right)\right) \right|^2 .$$

If the samples $W_v[k]$ are i.i.d. zero mean Gaussian distributed for all v and k, then minimizing $\mathcal{C}\left(\Psi_{\mathbf{p}_0}\right)$ yields the maximum likelihood estimates.

This nonlinear optimization problem is difficult to solve due to the large number of optimization variables and the highly oscillatory cost function $\mathcal{C}\left(\Psi_{\mathbf{p}_0}\right)$. This implies that optimization algorithms can get stuck in local minima very easily. Experiments with MATLAB's *lsqnonlin* optimization routine and random initialization values produced different results with large estimation errors. Only if the initialization values are chosen to be close to the true values, *lsqnonlin* converges to the global optimum. In order to solve this issue, we propose to separate the optimization problem into two sub-problems.

A. Sub-Problem 1: Path Gains and Delays at Reference Point

First, we consider only the measured received signal corresponding to $\mathbf{p}_0$. The coordinates of $\mathbf{p}_0$ need not be known. The cost function to be minimized is given by

$$\mathcal{C}_1\left(\{g_l(\mathbf{p}_0), \tau_l(\mathbf{p}_0)\}_{l=1}^{L(\mathbf{p}_0)}\right) = \sum_{k=-\frac{N}{2}}^{\frac{N}{2}-1} \left| R[k, \mathbf{p}_0] - S[k] \sum_{l=1}^{L(\mathbf{p}_0)} g_l(\mathbf{p}_0) \exp\left(-\imath \frac{2\pi k}{NT_s} \tau_l(\mathbf{p}_0)\right) \right|^2 . \tag{9}$$

This optimization problem still has a large number of variables, namely $2L(\mathbf{p}_0)$, and the cost function is highly oscillatory. However, there exist a number of iterative algorithms like the space-alternating generalized expectation-maximization (SAGE) algorithm [17], or the weighted Fourier transform and relaxation (WRELAX) algorithm [18], which are computationally efficient optimization algorithms providing very good results. The main idea of these algorithms is to transform the high-dimensional optimization problem in a series of one-dimensional optimization problems, which are then iteratively solved. In [19], the Hybrid-WRELAX algorithm is proposed, which is designed to minimize a highly oscillatory nonlinear least squares cost function. In this paper, we apply this algorithm to solve (9) and obtain estimates for the path gains and path delays when the transmitter is positioned at $\mathbf{p}_0$. These estimates are denoted by $\{\hat{g}_l(\mathbf{p}_0), \hat{\tau}_l(\mathbf{p}_0)\}_{l=1}^{L(\mathbf{p}_0)}$ and are used in the second sub-problem.

B. Sub-Problem 2: Linear Coefficients

In the second step, the remaining parameters (linear coefficients) are estimated, while the path gains and path delays are taken from the first sub-problem. The cost function to be minimized is given by

$$\mathcal{C}_2\left(\{\alpha_l,\beta_l,\gamma_l\}_{l=1}^{L(\mathbf{p}_0)}\right) = \sum_{v=1}^{V-1}\sum_{k=-\frac{N}{2}}^{\frac{N}{2}-1}\left|R\left[k,\mathbf{p}_v\right]-S\left[k\right]\sum_{l=1}^{L(\mathbf{p}_0)}\hat{g}_l\left(\mathbf{p}_0\right)\exp\left(-\imath\frac{2\pi k}{NT_s}\left(\hat{\tau}_l\left(\mathbf{p}_0\right)+\left[\alpha_l,\beta_l,\gamma_l\right]\left(\mathbf{p}_v-\mathbf{p}_0\right)\right)\right)\right|^2. \tag{10}$$

Note that we do not consider the measured received signal corresponding to $\mathbf{p}_0$ anymore and that only the relative displacements $\mathbf{p}_v-\mathbf{p}_0$ must be known. The linear coefficients α_l for all l are lower bounded by $-\frac{1}{c_0}$ and upper bounded by $\frac{1}{c_0}$ due to the bounds $-1\leq\frac{x_0+a}{\sqrt{(x_0+a)^2+(y_0+b)^2+(z_0+c)^2}}\leq 1$. The same bounds hold for β_l and γ_l. We apply MATLAB's *lsqnonlin* optimization routine using these bounds and obtain least squares estimates for the linear coefficients denoted by $\left\{\hat{\alpha}_l,\hat{\beta}_l,\hat{\gamma}_l\right\}_{l=1}^{L(\mathbf{p}_0)}$. All optimization variables are set to zero for the initialization of *lsqnonlin*. Experiments with random initialization values showed that always the same minimum $\mathcal{C}_2\left(\left\{\hat{\alpha}_l,\hat{\beta}_l,\hat{\gamma}_l\right\}_{l=1}^{L(\mathbf{p}_0)}\right)$ is obtained with the same values for $\left\{\hat{\alpha}_l,\hat{\beta}_l,\hat{\gamma}_l\right\}_{l=1}^{L(\mathbf{p}_0)}$. This indicates that *lsqnonlin* is able to find the global minimum.

V. Location Fingerprinting with Predicted Training Signals

A. Training Phase

Recall that the location fingerprinting parameters Θ_m have to be estimated during the training phase for all regions $m=1,2,\ldots,M$. We use J predicted training vectors and V measured training vectors for the estimation of Θ_m. The predicted signal at the j-th training point $\mathbf{p}_j^m$ is calculated by

$$r_{\text{pred}}\left[n,\mathbf{p}_j^m,\mathbf{p}_0^m\right]=\rho\sum_{l=1}^{L\left(\mathbf{p}_0^m\right)}\hat{g}_l\left(\mathbf{p}_0^m\right)s\left(nT_s-\hat{\tau}_l\left(\mathbf{p}_0^m\right)-\left[\hat{\alpha}_l,\hat{\beta}_l,\hat{\gamma}_l\right]\left(\mathbf{p}_j^m-\mathbf{p}_0^m\right)\right), \tag{11}$$

where ρ is an arbitrary scaling factor, which is chosen such that $r_{\text{pred}}\left[n,\mathbf{p}_j^m,\mathbf{p}_0^m\right]$ has unit energy. The reference point $\mathbf{p}_0^m$ is located within region m and it is ensured that $\mathbf{p}_j^m\notin\mathbb{P}^m$, i.e. a prediction point is not equal to a measurement point. The signals are processed according to the receiver front-end such that location fingerprint vectors are obtained. Depending on the stochastic model $f\left(\mathbf{y}|\Theta_m\right)$ the corresponding maximum likelihood parameter estimation

rule is applied to these $J+V$ training vectors which gives $\hat{\Theta}_m$. The location fingerprinting database also known as radio map consists of $\left\{\hat{\Theta}_1, \hat{\Theta}_2, \ldots, \hat{\Theta}_M\right\}$ and optionally the reference points $\left\{\mathbf{p}_0^1, \mathbf{p}_0^2, \ldots, \mathbf{p}_0^M\right\}$.

B. Localization Phase

During the localization phase, the anchor observes a location fingerprint vector $\mathbf{y}$ from an agent with unknown position (region), and evaluates the decision rule stated in (2). A classification error occurs whenever $\hat{m} \neq m$ and the current agent under test is located in region m. Many test positions within the whole surveillance area are evaluated in order to get a good estimate for $\mathcal{P}_e$ as defined in (1).

VI. Experimental Performance Analysis

In this section, we study the prediction accuracy and the achievable location fingerprinting performance with measured UWB channel impulse responses. The following results are obtained for a two-dimensional localization scenario, which implies that the agent is just allowed to move along the x-axis and y-axis and that $\hat{\gamma}_l = 0$ for all l. The reasons for this scenario are easier visualization and limitations of the measurement equipment. All position vectors have a constant z-coordinate from now on, i.e. $\mathbf{p}_0 = [x_0, y_0, z_0]^T$ and $\mathbf{p} = [x, y, z_0]^T$.

The prediction accuracy for a certain position $\mathbf{p}_j^m$ is defined in terms of the squared Euclidean distance between the true signal, i.e. the measured signal at high SNR, and the predicted signal given by

$$\mathcal{D}\left(\mathbf{p}_0^m, \mathbf{p}_j^m\right) = \sum_{n=0}^{N-1} \left| r\left[n, \mathbf{p}_j^m\right] - r_{\text{pred}}\left[n, \mathbf{p}_j^m, \mathbf{p}_0^m\right] \right|^2 .$$

Both signals $r\left[n, \mathbf{p}_j^m\right]$ and $r_{\text{pred}}\left[n, \mathbf{p}_j^m, \mathbf{p}_0^m\right]$ are normalized to unit energy, which implies that $0 \leq \mathcal{D}\left(\mathbf{p}_0^m, \mathbf{p}_j^m\right) \leq 4$. Recall that the normalization of $r_{\text{pred}}\left[n, \mathbf{p}_j^m, \mathbf{p}_0^m\right]$ to unit energy determines the scaling factor ρ in (11). In general, this scaling factor needs to be optimized such that the minimal squared Euclidean distance is achieved. We consider normalization to unit energy here, because the normalized predicted signals are used in the training phase of the location fingerprinting system. The overall prediction accuracy is measured with the mean prediction error $\mathcal{D}_e$ which is obtained by averaging $\mathcal{D}\left(\mathbf{p}_0^m, \mathbf{p}_j^m\right)$ over all prediction points within a given region and over all regions in the surveillance area according to

$$\mathcal{D}_e = \frac{1}{M} \sum_{m=1}^{M} \frac{1}{J} \sum_{j=1}^{J} \mathcal{D}\left(\mathbf{p}_0^m, \mathbf{p}_j^m\right).$$

In order to measure the performance of the optimization algorithms solving (9) and (10), we use the mean minimal costs $\bar{\mathcal{C}}_1$ and $\bar{\mathcal{C}}_2$, which are obtained by averaging the minimal costs from the optimization problems (9) and (10) over all regions in the surveillance area according to

$$\bar{\mathcal{C}}_1 = \frac{1}{M}\sum_{m=1}^{M} \mathcal{C}_1^m \left(\left\{ \hat{g}_l\left(\mathbf{p}_0^m\right), \hat{\tau}_l\left(\mathbf{p}_0^m\right) \right\}_{l=1}^{L\left(\mathbf{p}_0^m\right)} \right),$$

$$\bar{\mathcal{C}}_2 = \frac{1}{M}\sum_{m=1}^{M} \mathcal{C}_2^m \left(\left\{ \hat{\alpha}_l, \hat{\beta}_l, \hat{\gamma}_l \right\}_{l=1}^{L\left(\mathbf{p}_0^m\right)} \right).$$

For all following results we consider the same *assumed* number of paths for all regions, i.e. we let $L = L\left(\mathbf{p}_0^m\right)$ for all $\mathbf{p}_0^m$.

A. Anechoic Chamber Measurements

Channel impulse response measurements in an anechoic chamber[4] have been performed, in order to study the applicability of the regional channel model proposed in (8) in a controlled propagation environment.

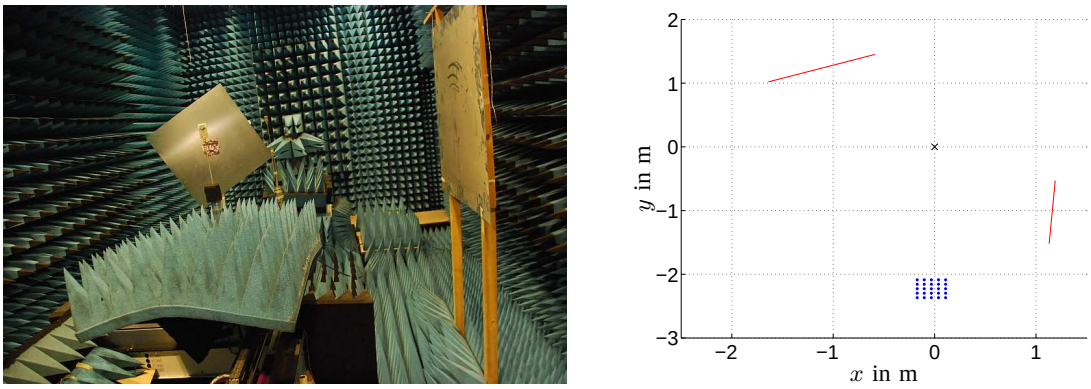

Figure 1. Photo of the measurement scenario with two metallic reflectors, fixed receive antenna, and transmit antenna mounted on a positioning device. The right plot shows the corresponding two-dimensional floor plan.

A photo of the measurement scenario and the corresponding two-dimensional floor plan are depicted in Figure 1. The propagation environment consists of two metallic reflectors, which are indicated with red lines in the floor plan. Hence, there exist $L_{\text{true}} = 3$ paths[5]. The black cross marks the position of the receive antenna (anchor) at the origin and the

[4]More details about these measurements can be found in Chapter 7 of [4].

[5]The two reflectors are placed such that multiple reflections do not exist.

blue dots mark some of the positions of the transmit antenna within the surveillance area. A positioning device is used, which is able to move the transmit antenna on a 0.01 m times 0.01 m grid over a surveillance area of 0.26 m times 0.26 m. The total number of measured channel impulse responses is $27 \cdot 27 = 729$. The surveillance area is quantized into $M = 4$ rectangular regions with dimensions 0.12 m times 0.12 m. Hence, there are $13 \cdot 13 = 169$ grid points in each region. The minimal distance between two grid points in adjacent regions is 0.02 m, i.e., a single grid line between the regions is disregarded. The surveillance area and the separation into regions are illustrated in Figure 2. The reference point $\mathbf{p}_0^m$ is chosen as the center point of region m. For example, the reference point of region 4 indicated by magenta cross markers is $\mathbf{p}_0^4 = [0.2, 0.2]^T$ m.

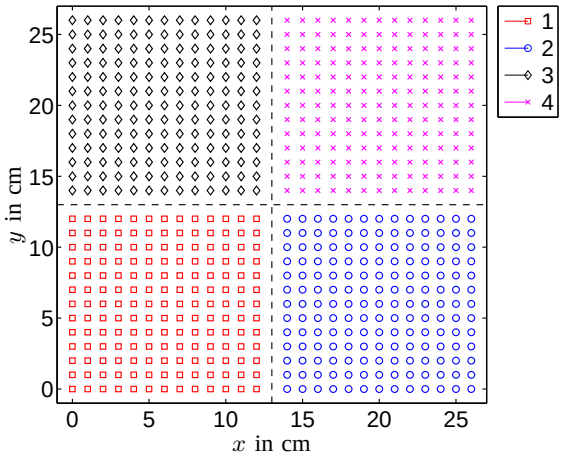

Figure 2. Surveillance area, measurement grid points, and the separation into $M = 4$ regions. Note the spacing of one grid line between adjacent regions.

Figure 3 depicts the measured and reconstructed received signals from the reference point of region 4. Furthermore, the difference between measured and reconstructed signals (error signal) is also shown. For visualization, the error signal is shifted by -0.25 on the ordinate. The measurement SNR is around 60 dB and the frequency band goes from 2 to 7 GHz. The reconstructed signal is obtained by applying the Hybrid-WRELAX algorithm to estimation problem (9) assuming $L = 3$ paths. It can be seen from visual inspection that the reconstruction is almost perfect. The minimal value of the cost function is $\mathcal{C}_1^4\left(\{\hat{g}_l\left(\mathbf{p}_0^4\right), \hat{\tau}_l\left(\mathbf{p}_0^4\right)\}_{l=1}^L\right) = 0.0275$. The error signal is largest right after the second path at $t \approx 8$ ns and the third path at $t \approx 15$ ns. The reason for these deviations might be a distortion of the transmit signal due to a frequency dependent reflection coefficient of the metallic objects.

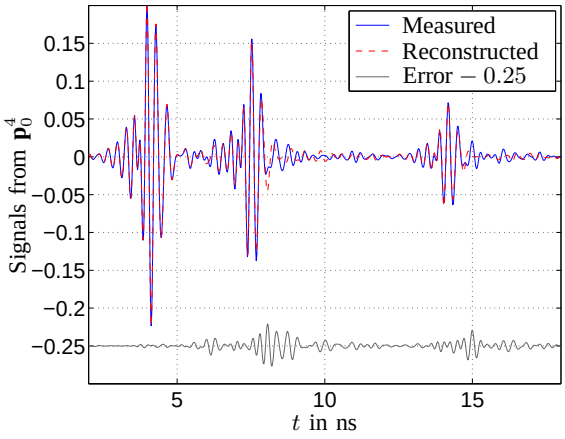

Figure 3. Measured, reconstructed and error signals from the reference point of region 4 denoted by $\mathbf{p}_0^4$. The reconstructed signal is obtained with Hybrid-WRELAX assuming $L = 3$ paths which results in $\mathcal{C}_1^4\left(\left\{\hat{g}_l\left(\mathbf{p}_0^4\right), \hat{\tau}_l\left(\mathbf{p}_0^4\right)\right\}_{l=1}^{L}\right) = 0.0275$.

1) Impact of Measurement Points: In this section, we investigate the impact of the coordinates of the measurement points on the prediction accuracy and the location fingerprinting performance. We consider $V = 3$ measurement points and define the following set

$$\mathbb{P}_1^m = \left\{\mathbf{p}_0^m, \mathbf{p}_0^m + \Delta \cdot [0.01, 0]^T, \mathbf{p}_0^m + \Delta \cdot [0, 0.01]^T\right\} \text{ with } \Delta \in \{-6, \ldots, -1, 1, \ldots, 6\},$$

such that the measurement points are the same in all four regions in relation to the reference point. The geometrical parameters are estimated with (9) and (10). The regional channel model from (8) is used to predict the signals from all grid points shown in Figure 2 except for the measurement points. These $J = 166$ predicted and $V = 3$ measured signals per region are used for maximum likelihood estimation of the location fingerprinting parameters Θ_m.

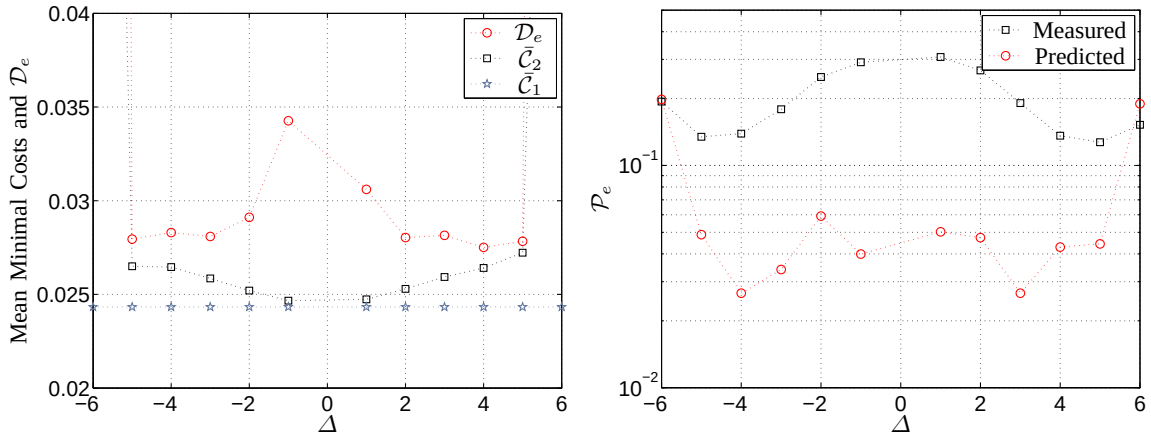

Figure 4. Performance results for $M = 4$, $L = 3$ and $\mathbb{P}_1^m = \left\{\mathbf{p}_0^m, \mathbf{p}_0^m + \Delta \cdot [0.01, 0]^T, \mathbf{p}_0^m + \Delta \cdot [0, 0.01]^T\right\}$.

In the left plot of Figure 4, we depict $\bar{\mathcal{C}}_1$, $\bar{\mathcal{C}}_2$ and $\mathcal{D}_e$ as function of Δ. First, note that $\bar{\mathcal{C}}_1$ is independent of Δ, since only the reference points are considered in (9). The very small value of $\bar{\mathcal{C}}_1$ indicates that approximation errors due to the input output relation in (3) are negligible for the considered reflectors and frequency band. Furthermore, it proves that the Hybrid-WRELAX algorithm provides an accurate solution to (9).

Second, the values for $\bar{\mathcal{C}}_2$ increase only slightly with $|\Delta|$ except for $|\Delta| = 6$. In this case, *lsqnonlin* converges only to a local optimum with a large error between estimated and true linear coefficients. In general, it can be said that farther apart measurement points lead to larger $\bar{\mathcal{C}}_2$. This behavior is due to the assumption of constant path gains and linear path delays which produces larger deviations as the distance to the reference point increases. However, the values of $\bar{\mathcal{C}}_2$ for $|\Delta| \leq 5$ are only slightly larger than $\bar{\mathcal{C}}_1$ which demonstrates that constant path gains and linear path delays are valid approximations. Moreover, these values show that *lsqnonlin* is able to provide accurate solutions to (10).

Third, it can be seen that $\mathcal{D}_e$ is only slightly larger than $\bar{\mathcal{C}}_1$ and $\bar{\mathcal{C}}_2$ for $|\Delta| \leq 5$ which finally proves the applicability of the regional channel model and the accuracy of the prediction method. As far as $\mathcal{D}_e$ is concerned, there is no clear dependency on Δ identifiable. Since $\bar{\mathcal{C}}_2$ is large for $|\Delta| = 6$, it is no surprise that $\mathcal{D}_e$ is also large in this case. We can show with the available measurements that received signals from agent positions up to a distance of 0.17 m to the reference point can be predicted very accurately with only $V = 3$ measurements. Longer prediction distances seem to be feasible.

In the right plot of Figure 4, we depict the location fingerprinting performance of a coherent UWB receiver (cf. Chapter 4 of [4] and [20]) in terms of $\mathcal{P}_e$ as function of Δ. We compare two $\mathcal{P}_e$ curves. The curve with the black square markers is obtained when only measured signals are used in the training phase. The average classification error probability is large and attains its smallest values for $|\Delta| \in \{4, 5\}$. Hence, the measurement points should be spread as evenly as possible within one region for smallest $\mathcal{P}_e$. The curve with the red circle markers is obtained when $V = 3$ measured signals are used to predict the signals from all other $J = 166$ grid points and all these $J + V$ signals are used in the training phase. The smallest achievable value of $\mathcal{P}_e$ is around 0.03 which constitutes are significant performance improvement (at least a factor five) compared to the measurement-only-curve. As for $\mathcal{D}_e$ there is also no clear dependency of $\mathcal{P}_e$ on Δ identifiable. The very large $\mathcal{P}_e$ for $|\Delta| = 6$ is again due to wrong estimates of the linear coefficients which cause an erroneous prediction.

2) Impact of Expected Number of Paths: In this section, we study the impact of L on the performance. We select two measurement sets with $V = 3$ given by

$$\mathbb{P}_2^m = \left\{\mathbf{p}_0^m, \mathbf{p}_0^m - [0.01, 0]^T, \mathbf{p}_0^m - [0, 0.01]^T\right\} \text{ i.e. } \Delta = -1,$$
$$\mathbb{P}_3^m = \left\{\mathbf{p}_0^m, \mathbf{p}_0^m + [0.03, 0]^T, \mathbf{p}_0^m + [0, 0.03]^T\right\} \text{ i.e. } \Delta = 3.$$

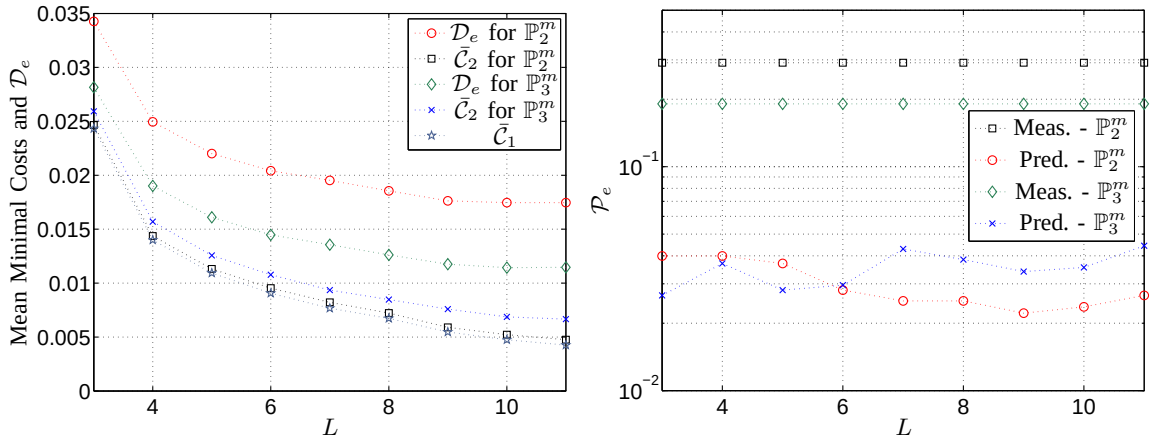

Figure 5. Results for $\mathbb{P}_2^m = \left\{\mathbf{p}_0, \mathbf{p}_0 - [0.01, 0]^T, \mathbf{p}_0 - [0, 0.01]^T\right\}$ and $\mathbb{P}_3^m = \left\{\mathbf{p}_0, \mathbf{p}_0 + [0.03, 0]^T, \mathbf{p}_0 + [0, 0.03]^T\right\}$.

Figure 5 depicts the performance results as function of an assumed number of paths L. It can be seen that $\bar{\mathcal{C}}_1$, $\bar{\mathcal{C}}_2$ and $\mathcal{D}_e$ decrease by increasing L. Hence, the multipath approximation of the measured (true) signals with (3) becomes more accurate as L is increased. One reason for the increased approximation accuracy with larger L might be the compensation of pulse distortions due to frequency dependent interactions.

From the right plot of Figure 5, it can be seen that $\mathcal{P}_e$ using predicted training signals is essentially independent of L. This means that the increased approximation accuracy does not have a significant impact on the localization performance.

3) Classification Results: In this section, we have a closer look on the classification results. We consider measurement set $\mathbb{P}_2^m$ from above and set $L = 9$. According to Figure 5 this yields the smallest value of $\mathcal{P}_e \approx 0.02$. If only the $V = 3$ measured signals are used for training, then $\mathcal{P}_e \approx 0.3$ is achieved in this case. Figure 6 depicts the corresponding classification results. All measured signals from all grid points are used as observations during the localization phase. The training phase is either done with only $V = 3$ measured signals per region (cf. left plot) or with $J = 166$ predicted and $V = 3$ measured signals per region (cf. right plot). The markers indicate the classification results, i.e. $\hat{m}$. For example, magenta cross markers

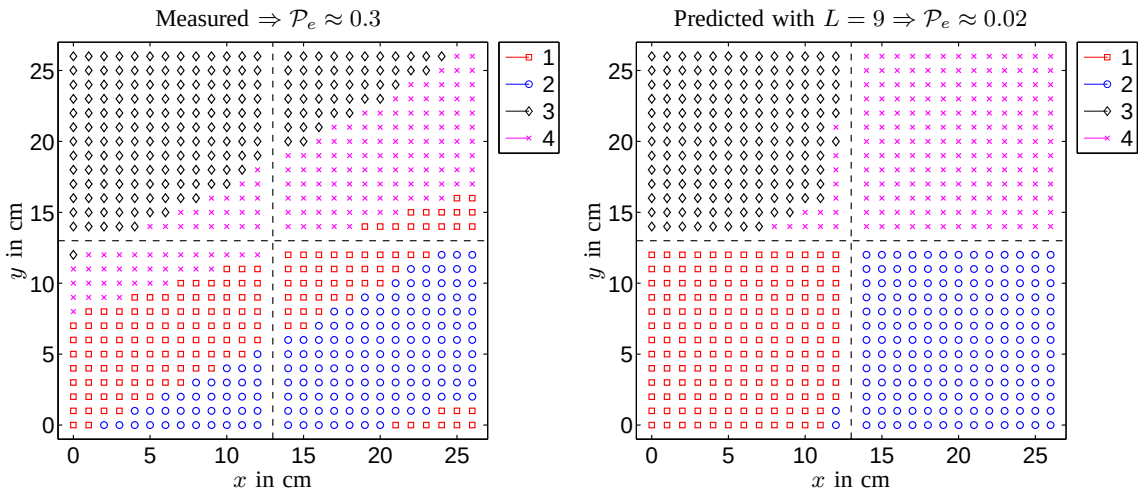

Figure 6. Classification results for $L = 9$ and $\mathbb{P}_2^m = \{\mathbf{p}_0^m, \mathbf{p}_0^m - [0.01, 0]^T, \mathbf{p}_0^m - [0, 0.01]^T\}$.

indicate that observations from these grid points are classified to region 4. It can be seen from the left plot of Figure 6 that the classification into the prescribed rectangular regions (cf. Figure 2) fails with only three measured signals for training. However, the classification results are surprisingly coherent and form regions with specific shapes. It is conjectured that these shapes are determined by the physical nature of the propagation channel, i.e. by the geometrical constellation of reflectors, transmitter and receiver. It is possible to impose rectangular shaped regions, as required by the location fingerprinting application, by utilizing predicted signals from all grid points for training. The corresponding results are shown in the right plot of Figure 6. The rare classification errors happen only at the region borders. It can be concluded that the proposed prediction scheme offers the additional possibility to shape the regions based on the selection of prediction points $\mathbf{p}_j^m$.

B. Office Environment Measurements

In this section, we evaluate the proposed prediction method with UWB channel impulse response measurements obtained in an office environment at IMST GmbH, Kamp-Lintfort, Germany. More details about these measurements can be found in [21] and [22]. We consider a surveillance area of 1.10 m times 0.26 m which is separated into $M = 16$ regions with dimensions 0.12 m times 0.12 m. As in Section VI-A, the grid spacing is 0.01 m in x-direction and in y-direction. The minimal distance between two grid points in adjacent regions is 0.02 m. Essentially, four blocks as depicted in Figure 2 are stacked together along the x-axis to form the surveillance area.

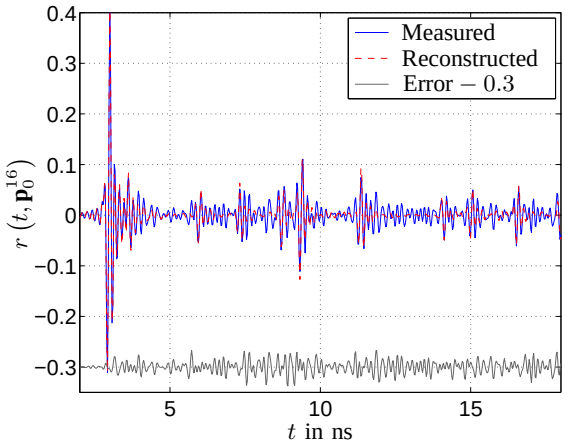

Figure 7. Measured, reconstructed and error signals from $\mathbf{p}_0^{16}$. The reconstructed signal is obtained with Hybrid-WRELAX assuming $L = 15$ paths which gives $\mathcal{C}_1^{16}\left(\left\{\hat{g}_l\left(\mathbf{p}_0^{16}\right),\hat{\tau}_l\left(\mathbf{p}_0^{16}\right)\right\}_{l=1}^{L}\right) = 0.14$.

Figure 7 depicts the measured, reconstructed and error signals, when the transmit antenna is placed on the reference point of region 16. For visualization, the error signal is shifted by -0.3 on the ordinate. The measurement SNR is around 50 dB and the observed frequency band goes from 1 to 11 GHz. The reconstructed signal is obtained by applying the Hybrid-WRELAX algorithm to (9) assuming $L = 15$ paths, which results in $\mathcal{C}_1^{16}\left(\left\{\hat{g}_l\left(\mathbf{p}_0^{16}\right),\hat{\tau}_l\left(\mathbf{p}_0^{16}\right)\right\}_{l=1}^{L}\right) = 0.14$. The reconstruction error is larger in the office environment than in the anechoic chamber (cf. Figure 3), but it is still reasonably small. Especially the reconstruction of strong multipath components like those at $t \approx 9$ ns and $t \approx 12$ ns is very accurate.

1) Impact of Measurement Points: In addition to $\mathbb{P}_1^m$ (cf. Section VI-A), we consider the following sets of measurement points

$$\mathbb{P}_4^m = \left\{\mathbf{p}_0^m, \mathbf{p}_0^m + \Delta\cdot[0.01, 0.01]^T, \mathbf{p}_0^m + \Delta\cdot[-0.01, 0.01]^T, \mathbf{p}_0^m + \Delta\cdot[0.01, -0.01]^T, \mathbf{p}_0^m - \Delta\cdot[0.01, 0.01]^T\right\}$$

with $V = 5$ and $\Delta \in \{1, \ldots, 6\}$.

Figure 8 depicts the prediction and location fingerprinting performance as function of Δ assuming $L = 15$ paths. The curves have the same meaning as in Figure 4 and similar observations as for the anechoic chamber results can be made. Increasing $|\Delta|$ results in larger $\bar{\mathcal{C}}_2$, $\mathcal{D}_e$ and $\mathcal{P}_e$. The closest measurement points, i.e. $|\Delta| = 1$, lead to the best overall prediction accuracy (smallest $\mathcal{D}_e$) and to the best location fingerprinting performance (smallest $\mathcal{P}_e$). This holds for $\mathbb{P}_1^m$ as well as for $\mathbb{P}_4^m$. The reason for this behavior is the dense spacing of multipath components, which causes the *path pairing* problem: If two paths, which are caused by two different interacting objects, have almost equal path delays at the reference

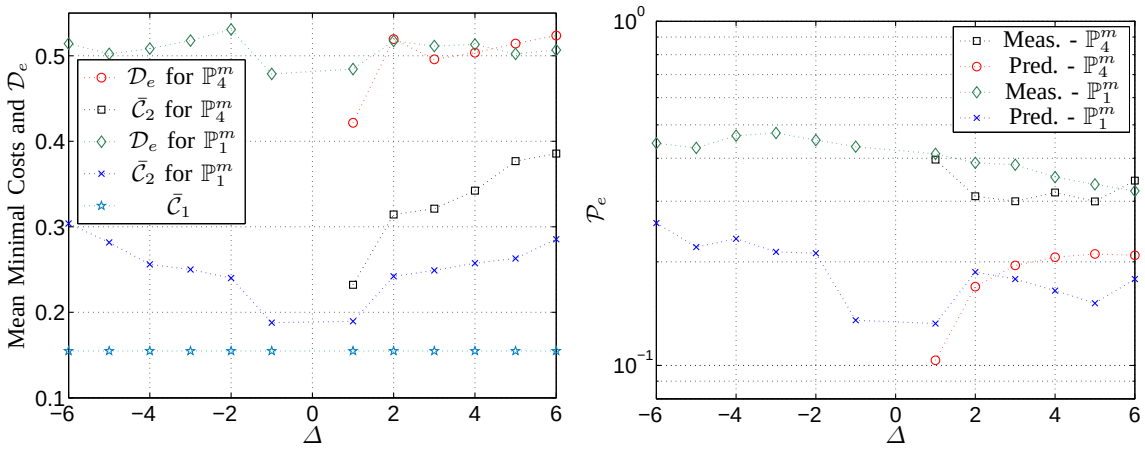

Figure 8. Performance results for $M = 16$, $L = 15$, $\mathbb{P}_1^m$ and $\mathbb{P}_4^m$ as function of Δ.

point, then the probability is high that these two paths are confused during the estimation of the linear coefficients. In other words, the cost function (10) has a local minimum which is very close to the global minimum, but the corresponding linear coefficient estimates are totally different.

If the number of measurement points is increased from $V = 3$ for $\mathbb{P}_1^m$ to $V = 5$ for $\mathbb{P}_4^m$, performance gains in terms of $\mathcal{D}_e$ and $\mathcal{P}_e$ are only visible for $|\Delta| = 1$. By using predicted signals based on measurement set $\mathbb{P}_4^m$ with $\Delta = 1$, the location fingerprinting performance can be improved from $\mathcal{P}_e \approx 0.4$ to $\mathcal{P}_e \approx 0.1$ by a factor of four. Without prediction the smallest achievable $\mathcal{P}_e$ is 0.3 which implies a minimal performance improvement by a factor of three.

2) Impact of Expected Number of Paths: In general, the number of multipath components $L(\mathbf{p})$ depends on the position of the transmit antenna and is unknown. In order to simplify the estimation problems, we assume a fixed L for all antenna positions within the surveillance area. This is of course a simplification. In future work, we plan to estimate $L(\mathbf{p})$ from measured channel impulse responses as well.

The more multipath components are used to model the channel impulse response, the more channel model parameters must be estimated. Hence, the problem of overfitting arises, which is well known in the context of e.g. neural networks or statisctical learning theory. If models with many parameters are used to describe measured data, this has a negative impact on the generalization property of the model. Generalization is in analogy to prediction considered in the problem at hand. Hence, it is expected that the costs of both estimation sub-problems

- $\bar{\mathcal{C}}_1$ and $\bar{\mathcal{C}}_2$ - decrease as L increases but at the same time that the prediction accuracy and consequently the location fingerprinting performance - $\mathcal{D}_e$ and $\mathcal{P}_e$ - degrade.

For the following results, we select the measurement points

$$\mathbb{P}_5^m = \left\{\mathbf{p}_0^m, \mathbf{p}_0^m + [0.01, 0.01]^T, \mathbf{p}_0^m + [-0.01, 0.01]^T, \mathbf{p}_0^m + [0.01, -0.01]^T, \mathbf{p}_0^m - [0.01, 0.01]^T\right\}.$$

According to Figure 8 these measurement points yield $\mathcal{P}_e = 0.1$, when $L = 15$ multipath components are assumed. Figure 9 depicts performance results as function of L. As ex-

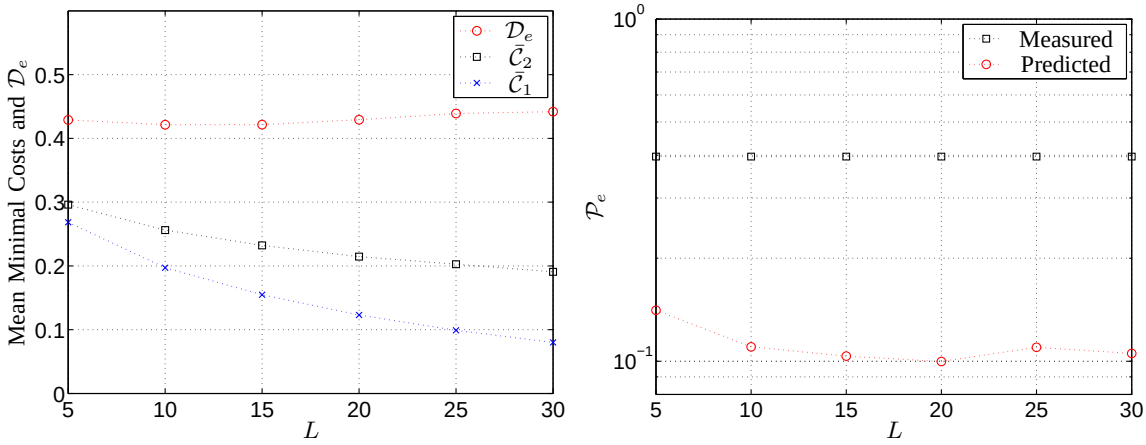

Figure 9. Performance results for $M = 16$, $V = 5$ and $\mathbb{P}_5^m$.

pected, $\bar{\mathcal{C}}_1$ and $\bar{\mathcal{C}}_2$ decrease monotonously with L. The situation is, however, different for $\mathcal{D}_e$. First a slight improvement and after $L = 15$ a slight degradation is visible. Similar observations can be made from the results for $\mathcal{P}_e$. The location fingerprinting performance first improves until $L = 20$, but then degrades again. These observations are in accordance with the aforementioned overfitting problem. However, overfitting is not the only reason for performance degradation. The input output relation (3) is based on geometrical optics, which implies that not all multipath components are properly modeled and predictable. There are always components in a measured channel impulse response, which can be only modeled stochastically. Another reason for performance degradation is the aforementioned path paring problem.

Nevertheless, these experimental results confirm that there exist at least some predictable multipath components like reflections from walls, such that a significant improvement of the location fingerprinting performance is achievable by using predicted channel impulse responses for training.

VII. Discussion and Conclusions

The main disadvantage of location fingerprinting approaches in comparison to conventional position location schemes is the need for a training phase posing a significant measurement effort. The work in this paper shows a method how to alleviate this drawback by exploiting the very high temporal resolution of the wireless propagation channel of UWB signals. We present a parameterized regional channel model, which is suited to predict received RF signals based on only very few measurements. The predicted signals are used as artificial training data by the location fingerprinting system to learn the *initial* location fingerprinting parameters [4], [23]. During the localization phase, many location fingerprints containing additional information about the propagation environment are observed and can be utilized to learn the parts of the parameters Θ_m, which are caused by unpredictable propagation effects. Such a scheme would constantly improve over time assuming a static propagation environment and, moreover, would be able to cope with small changes of the propagation environment by constantly adapting Θ_m utilizing new observations and forgetting older observations.

An experimental analysis demonstrates the achievable prediction and localization performance in a controlled propagation environment as well as in a typical office environment. The prediction results for the anechoic chamber are very promising and prove the accuracy of all approximations and chosen estimation algorithms. Moreover, these results confirm the applicability and validity of the regional channel model. The prediction accuracy drops in the office environment with dense multipath propagation. The path pairing problem is identified as the main error source. Many and densely spaced multipaths cause erroneous estimates of the channel model parameters and, consequently, wrong predictions as well as classification errors. However, the experimental performance results for the office environment demonstrate that there exist also in dense multipath channels predictable components which can be utilized to improve the training phase. A thorough analysis of the path pairing problem and the development of countermeasures are planned for future work. A natural way to mitigate path pairing errors would be to increase the temporal resolution, i.e., to increase the signal bandwidth.

APPENDIX

RELATION OF LINEAR COEFFICIENTS TO THE ANGLE OF DEPARTURE

We restrict the exposition to the two-dimensional Euclidean space for the sake of visualization and investigate the relationship between α_l and β_l and the angle of departure ϕ_l of the l-th multipath component. The path index l is dropped for notational convenience.

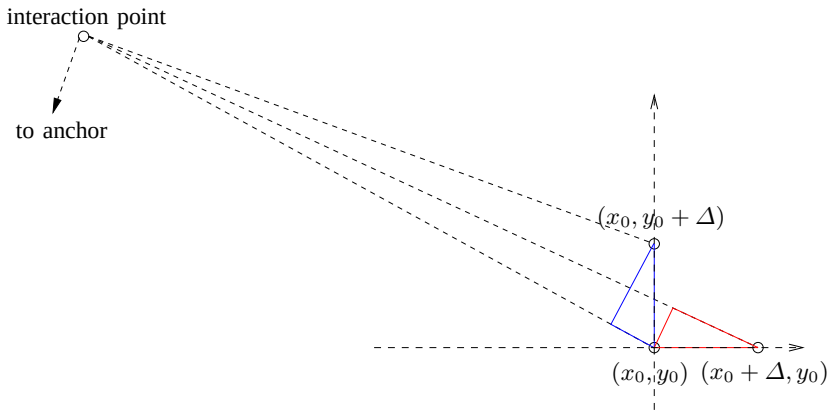

Figure 10. Propagation paths from agent via interacting object to anchor.

Figure 10 depicts the propagation paths from three measurement points denoted by (x_0, y_0), $(x_0 + \Delta, y_0)$, and $(x_0, y_0 + \Delta)$ via an interaction point to the anchor. The time required for the signal from (x_0, y_0) to travel to the anchor is denoted by $\tau(x_0, y_0)$. Figure 11 depicts a

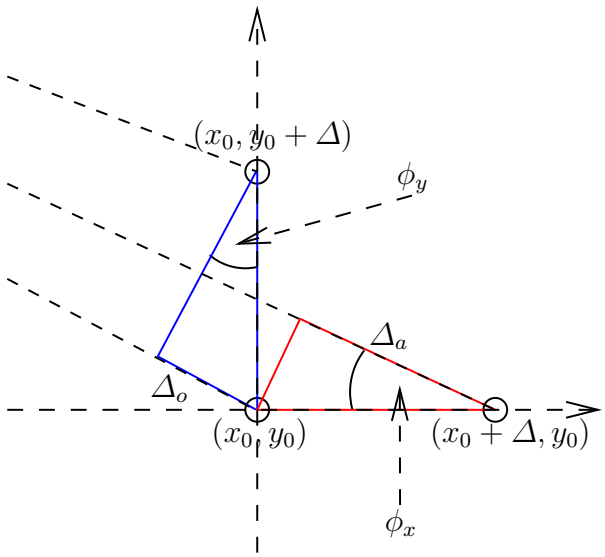

Figure 11. Angles of departure ϕ_x and ϕ_y.

close up of Figure 10. The two right-angled triangles define the angles of departure ϕ_x and

ϕ_y with respect to x-axis and y-axis according to

$$\cos\phi_x = \frac{\Delta_a}{\Delta} \text{ and } \sin\phi_y = \frac{\Delta_o}{\Delta},$$

where Δ is the length of the hypotenuses of these triangles. The adjacent leg of ϕ_x has the length Δ_a and the opposite leg of ϕ_y has the length Δ_o.

If the distance from (x_0, y_0) to the interacting object is large compared to Δ, the plane wave assumption can be invoked, which states that the three propagation paths depicted in Figure 10 and Figure 11 can be treated as parallel. In the close up in Figure 11, it can be seen that these paths are indeed approximately parallel. Accordingly, the lengths Δ_a and Δ_o are given by

$$\Delta_a = c_0\left(\tau(x_0+\Delta, y_0) - \tau(x_0, y_0)\right) \text{ and } \Delta_o = c_0\left(\tau(x_0, y_0) - \tau(x_0, y_0+\Delta)\right).$$

Hence, assuming plane waves yields $\phi = \phi_x = \phi_y$ and

$$\cos\phi = \cos\phi_x = \frac{c_0\left(\tau(x_0+\Delta, y_0) - \tau(x_0, y_0)\right)}{\Delta},$$
$$\sin\phi = \sin\phi_y = \frac{c_0\left(\tau(x_0, y_0) - \tau(x_0, y_0+\Delta)\right)}{\Delta}.$$

Another consequence of the plane wave assumption is that the linear approximation of the path delays in (6) becomes exact. This can be seen from Figure 11 and the equation

$$\tau(x,y) = \tau(x_0,y_0) + \underbrace{\frac{\cos\phi}{c_0}}_{\alpha}(x-x_0) + \underbrace{\left(-\frac{\sin\phi}{c_0}\right)}_{\beta}(y-y_0).$$

The relationship between α and β and the angle of departure ϕ follows as

$$\alpha = \frac{\cos\phi}{c_0} = \frac{\tau(x_0+\Delta, y_0) - \tau(x_0, y_0)}{\Delta} \text{ and } \beta = -\frac{\sin\phi}{c_0} = \frac{\tau(x_0, y_0+\Delta) - \tau(x_0, y_0)}{\Delta}.$$

It can be concluded that the plane wave assumption, commonly applied for angle of departure or angle of arrival estimation with antenna arrays, is in analogy to the linear approximation of the path delays proposed in (6). In literature there exist a lot of algorithms, which estimate ϕ with antenna arrays. Those could be also utilized for the estimation of α and β.

REFERENCES

[1] F. Gustafsson and F. Gunnarsson, "Mobile positioning using wireless networks: Possibilities and fundamental limitations based on available wireless network measurements," *IEEE Signal Processing Magazine*, vol. 22, pp. 41–53, July 2005.

[2] G. Sun, J. Chen, W. Guo, and K. J. R. Liu, "Signal processing techniques in network-aided positioning: A survey of state-of-the-art positioning designs," *IEEE Signal Processing Magazine*, vol. 22, pp. 12–23, July 2005.

[3] K. Kaemarungsi, *Design of indoor positioning systems based on location fingerprinting technique*. Ph.D. Thesis, University of Pittsburgh, 2005.

[4] C. Steiner, *Location Fingerprinting for Ultra-Wideband Systems. The Key to Efficient and Robust Localization*. Ph.D. Thesis, ETH Zürich, No. 19147, 2010.

[5] S. Gezici, Z. Tian, G. Giannakis, H. Kobayashi, A. Molisch, H. Poor, and Z. Sahinoglu, "Localization via ultra-wideband radios: A look at positioning aspects for future sensor networks," *IEEE Signal Processing Magazine*, vol. 22, pp. 70–84, July 2005.

[6] S. Gezici and H. Poor, "Position estimation via ultra-wide-band signals," *Proceedings of the IEEE*, vol. 97, pp. 386–403, February 2009.

[7] R. Moses, D. Krishnamurthy, and R. Patterson, "A self-localization method for wireless sensor networks," *EURASIP Journal on Applied Signal Processing*, vol. 2003, pp. 348–358, March 2003.

[8] M. Brunato and R. Battiti, "Statistical learning theory for location fingerprinting in wireless LANs," *Computer Networks and ISDN Systems*, vol. 47, no. 6, pp. 825–845, 2005.

[9] C. M. Bishop, *Pattern Recognition and Machine Learning*. Springer, 1 ed., October 2007.

[10] S. M. Kay, *Fundamentals of Statistical Signal Processing: Detection Theory*, vol. 2. Prentice Hall PTR, January 1998.

[11] A. Molisch, "Ultra-wide-band propagation channels," *Proceedings of the IEEE*, vol. 97, pp. 353–371, February 2009.

[12] A. Saleh and R. Valenzuela, "A Statistical Model for Indoor Multipath Propagation," *IEEE Journal on Selected Areas in Communications*, vol. 5, no. 2, pp. 128–137, 1987.

[13] D. McNamara, C. Pistorius, and J. Malherbe, *Introduction to the Uniform Geometrical Theory of Diffraction*. Artech House, 1990.

[14] T. S. Rappaport, *Wireless Communications: Principles and Practice*. Prentice Hall PTR, 2 ed., December 2001.

[15] E. M. Lavely, Y. Zhang, E. H. Hill, Y. san Lai, P. Weichman, and A. Chapman, "Theoretical and experimental study of through-wall microwave tomography inverse problems," *Journal of the Franklin Institute*, vol. 345, no. 6, pp. 592 – 617, 2008.

[16] G. Hickman and J. L. Krolik, "A graph-theoretic approach to constrained floor plan estimation from radar measurements," *IEEE Transactions on Signal Processing*, vol. 57, pp. 1877–1888, May 2009.

[17] B. Fleury, M. Tschudin, R. Heddergott, D. Dahlhaus, and K. Ingeman Pedersen, "Channel parameter estimation in mobile radio environments using the SAGE algorithm," *IEEE Journal on Selected Areas in Communications*, vol. 17, pp. 434–450, March 1999.

[18] J. Li and R. Wu, "An efficient algorithm for time delay estimation," *IEEE Transactions on Signal Processing*, vol. 46, pp. 2231–2235, August 1998.

[19] R. Wu and J. Li, "Time-delay estimation via optimizing highly oscillatory cost functions," *IEEE Journal of Oceanic Engineering*, vol. 23, pp. 235 –244, jul 1998.

[20] C. Steiner, F. Althaus, F. Troesch, and A. Wittneben, "Ultra-wideband geo-regioning: A novel clustering and localization technique," *EURASIP Journal on Advances in Signal Processing*, p. 13, January 2008.

[21] J. Kunisch and J. Pamp, "Measurement results and modeling aspects for the UWB radio channel," in *IEEE Conference on Ultra Wideband Systems and Technologies, UWBST*, pp. 19–23, May 2002.

[22] J. Kunisch and J. Pamp, "An ultra-wideband space-variant multipath indoor radio channel model," in *IEEE Conference on Ultra Wideband Systems and Technologies, UWBST*, pp. 290 – 294, Sept. 2003.

[23] C. Steiner and A. Wittneben, "Clustering of wireless sensors based on ultra-wideband geo-regioning," in *Asilomar Conference on Signals, Systems, and Computers*, pp. 1345–1349, November 2007.

Christoph Steiner Christoph Steiner received the Dipl.-Ing. degree in telematics from Graz University of Technology, Austria, in 2005 with distinction, and the Ph.D. degree in electrical engineering from the Swiss Federal Institute of Technology (ETH) Zurich in 2010. Since October 2010 he is with Infineon Technologies Austria AG. His research interests are in the field of signal processing for wireless communication and position location.

Armin Wittneben Armin Wittneben received the Dipl.-Ing. and the Dr.-Ing. (PhD) degree in Electrical Engineering from the Technical University of Darmstadt in 1983 and 1989 respectively. From 1989 to 1998 he was with the research organization of ASCOM/Switzerland and in charge of the Radio Communications research department. In 1997 he completed the habilitation thesis „Diversity schemes in mobile communications“. In 1998 he accepted a position as Full Professor of Communications at the Saarland University, Saarbrücken (Germany). Since 2002 he has been Full Professor of Wireless Communications at ETH Zurich and head of the Communication Technology Laboratory. His research interests comprise the Physical and the Data Link Layer of Wireless Communication Systems as well as selected aspects of the Network Layer. Currently he is focusing on (i) cooperative signaling, signal processing and relaying in short range and cellular wireless systems, (ii) Ultra Wideband/Ultra Low Power Wireless, (iii) nonlinear MIMO and (iv) blind position location.